

Synthesis and Magnetic Performance of Gadolinium Powder Produced with Rotating Disk Atomization

Sam Wolf^{1,2}, Trevor M. Riedemann¹, John Barclay³, Jamie Holladay⁴, Iver E. Anderson^{1,2}, Jun Cui^{1,2}

1. Materials Science and Engineering Division, Ames Laboratory, Ames, IA 50011
2. Department of Materials Science and Engineering, Iowa State University, Ames, IA 50011
3. Emerald Energy NW, LLC, Bothell, WA 98012
4. Energy and Environment Directorate, Pacific Northwest National Laboratory (USDOE), Richland, WA 99354

Tel: 515.294.0973, e-mail: sejwolf@iastate.edu

Abstract: Spherical powder is key for achieving good heat transfer and maintaining low pressure drop for heat transfer fluid in magnetocaloric regenerator. Obtaining relatively large spherical powder of rare earth metals that are extremely sensitive to oxygen is challenging. Comparing to gas atomization and plasma rotating electrode methods, rotating disk atomization (RDA) method is more robust for obtaining a small amount of powder with a short turn-around time, thereby, more suitable for research and development of new magnetocaloric materials. In this work, commercially bulk gadolinium was successfully atomized to produce spherical powder in the targeted 150-250 μm range. The obtained powder exhibited the expected magnetocaloric performance with a maximum change of magnetic entropy of 12.1 J/kg K and a maximum adiabatic temperature change of 12.8 K with an applied magnetic field of 7 T.

1 Introduction

In recent years, the pursuit of magnetic refrigeration has generated much research in magnetocaloric materials. Utilizing the thermodynamic phenomenon of the magnetocaloric effect (MCE), magnetic refrigeration has both theoretically and experimentally shown a cooling cycle

with efficiencies surpassing conventional refrigeration techniques[1], sparking an interest in designing commercially viable systems to realize this technology.

An active magnetic regenerator (AMR) is used to achieve wider cooling ranges beyond the adiabatic temperature change produced in the most powerful magnetocaloric materials such as Gadolinium. AMRs work on the premise of cycling the magnetocaloric material in and out of an externally applied magnetic field producing alternating periods of heating and cooling. The heating or cooling periods in the refrigeration cycle are completed when heat from or to the magnetic material is transferred via a reciprocating flow of heat-transfer fluid [2]. Therefore, the magnetocaloric material must take on a permeable form to encourage efficient regenerative heat exchange. Four principles are important in the design of high-performance AMRs and the selection of size, shape and architecture of the magnetocaloric materials: high surface area for convective heat transfer between the fluid and the solid; low pressure drop from the heat transfer fluid flow; low longitudinal thermal conduction including eddy diffusivity mixing; and low eddy current heating. The prototype AMR system for which the present material research was conducted used a powder-bed geometry for the magnetocaloric materials to achieve excellent heat transfer between the heat-transfer fluid and the working solid refrigerant. Spherical powder with a diameter of 150-250 micron was used to balance the low pressure drop and high thermal contact area.

The prototype uses identical, opposing dual AMRs with a cold heat exchanger between them in a piston configuration. A detailed description of the prototype system can be found in references [3-5]. While the recent AMRs under development use multiple layers of different magnetocaloric materials with sequentially lower Curie temperatures to extend the temperature spans of the AMR from about 280 K towards 20 K, the forthcoming discussion focuses on the first layer material, gadolinium. Gadolinium has been well studied for use in magnetic refrigeration as its ferromagnetic ordering transition (T_{Curie}) at 294 K produces a large MCE lending itself to near

room temperature refrigeration [6]. The measured peak adiabatic temperature change is reported in the literature to be around 11.0 K from an applied magnetic induction change of 5 T and 3.6 K at 1 T; and the peak change of total entropy is approximately 10.5 J/kg K at 5 T and 3.25 J/kg K at 1 T [7-9].

When choosing the method for producing this 200 μm size spherical metal powders for developing cryogenic magnetocaloric applications, several important factors to be considered are turn-around time, powder performance and cost. Turn-around time is important because compositional space of cryogenic magnetocaloric materials is not well charted. Prolific compositional refinement requires the powder-making method to be nimble and capable of reliably producing small batches of powder with narrow size distribution and, when alloys are needed, controlled composition. Gas atomization can produce a large quantity of spherical powder but typically the resulting size distribution is wide, the turn-around time is long and the batch size is limited to tens of kilograms and above, which will inevitably lead to a large stock-pile of expensive rare-earth powders that may or may not be able to find a future use. Similarly, a plasma rotating electrode process also suffers from long turn-around time. It requires the feedstock materials to be first cast into a large ingot then machined into a rod with precise dimensions necessary for the high rotation speed during the plasma eroding process, which in itself is a project for each of the candidate compositions. Ball-milling processes are a common method for producing rare-earth metal powders for permanent magnet applications. The method has short turn-around time. It is cost effective and clean. Unfortunately, ball-milled powder is not spherical and may result in some amorphous powder. The irregular particle shapes increases packed-regenerator porosities from ~36 % to as high as ~50% that reduce specific refrigerant volume of the regenerator and increase turbulence in the flow of the heat-exchange fluid, which degrades AMR performance.

Centrifugal atomization off a rotating disk was chosen to produce spherical rare earth powders with a relatively large diameter, i.e. 150-250 micron. This technique is advantageous as

powder produced with centrifugal atomization can be highly spherical with a narrow size distribution, tunable to reach a specific powder diameter. Centrifugal atomization has been used to produce fine powders of metals, including intermetallic lanthanide materials [10]. This technique employs centrifugal forces generated with a high-speed rotating disk to break apart a flow of molten metal poured onto the disk into droplets. This type of high-yield, small-batch process is ideal for quickly producing powders from various exploratory rare-earth metals and alloys. The work reported in this article uses gadolinium metal as the baseline material to develop and calibrate the synthesis process. In addition to gadolinium, 8 more rare earth alloys were prepared using the developed method. The characterized properties of those new alloys and produced powders will be published in a different article.

2 Material and Methods

2.1

Atomization System Design

Figure 1 shows a schematic of the rotating disk atomization (RDA) system used to produce the gadolinium powder at the Ames Laboratory. This system found previous use in the production of Ca powder as described by Tian et. al. [11], and was modified for production of rare earth powders. The system is enclosed to provide vacuum capability that can be backfilled with an argon atmosphere essential to preventing oxidization of the rare earth charge material. A Gd charge is loaded into a Ta crucible positioned above the disk. The solid charge is then melted by the surrounding induction coil and, with the disk rotating at the operational speed, the stopper rod plugging the pour spout is removed, and the molten charge is poured on to the rotating disk.

The disk assembly consists of a Ta disk atop a ceramic base coupled to an electric motor to drive rotation at about 8,000 RPM. The thin (0.76 mm) Ta disk is quickly heated upon contact with the molten charge material while the ceramic base prevents significant thermal transfer, thus reducing buildup of solidified charge metal on the disk. Centered atop the disk is a conical

tantalum pin, 9.5 mm in diameter at the base and 8.2 mm tall. The stream of liquid metal pours onto the pin which helps to evenly spread the flow over the surface of the disk. Centrifugal force drives the liquid to the spinning disk edge where the melt forms ligaments, which break apart into droplets and subsequently solidify into spherical powder.

The RDA at Ames employs a co-rotating quench bath highlighted in the insert of *Figure 1*. An external motor rotates the bath forcing the silicone oil (KJ Lesker 704CA) up the sides of the bath and producing a vertical quench wall approximately 3 cm thick. The quench fluid allows us to produce powder from potentially flammable materials, such as Re and Ca, by safely capturing them in the fluid. Additionally, the quench bath captures and solidifies larger drops or liquid fragments that are too massive to complete solidification before impinging upon the fluid.. Whereas other centrifugal atomization techniques require long distances to allow the metal to cool in atmosphere, a rotating quench bath used with centrifugal atomization allows the RDA system to be contained in a two-foot diameter chamber. The positive aspect of this design is it is well suited for lab scale work, while the drawback is that flake shaped powder may be produced when liquid metal is quenched in the bath. That flake must then be separated from the desired spherical powder.

There are several key parameters including system design and materials properties which dictate the forces and breakup of the liquid metal and, ultimately, the powder size. Champagne and Angers developed an empirical formula used to predict mean particle size (d_{50}) in centrifugal atomization [12].

$$d_{50} = \frac{3.65Q^{0.06}}{\omega D^{0.58}} \left(\frac{\gamma}{\rho}\right)^{0.46} \quad (\text{Eq. 1})$$

where Q is the flow rate of the liquid metal, ω is the rotational speed of the disk, D is the disk diameter, γ is the liquid metal surface tension, and ρ is the liquid metal density. Using this basis,

the particle size distribution can be tuned by changing run parameters such as disk diameter and speed, superheat (surface tension), and crucible orifice diameter (flow rate).

For the atomization of pure Gd in the RDA, a 41 mm diameter tantalum disk was used spun at 8,000 RPM. The Gd was induction melted and heated 120 °C above its melting temperature (1313 °C) and poured out of the Ta crucible spout orifice, 1.6 mm in diameter, by raising a stopper rod insert in the orifice. Using these parameters and properties of liquid Gd [13] with the Champagne-Angers equation, a d_{50} of 207 μm was predicted.

For each atomization run, a 1,300-1,500 g charge of Gd was loaded into the crucible. After atomization the metal powder was collected from the quench bath, rinsed in solvent to remove excess oil, and dried in vacuum before metallographic, physical, and magnetic characterization.

2.2

Materials

While numerous publications have shown that magnetocaloric performance of Gd suffers with decreasing purity [6, 14-16], however, the quantity of powder required for the AMR made it more economically viable if a commercial grade Gd stock can be substituted for higher purity metal. This work used commercially available Gd metal from HEFA Rare Earth Canada Ltd (reported minimum purity 99.5 wt% total rare earth metal (TREM), 99.99 wt% Gd/TREM). The specific reported impurities from the supplier are reported in *Table 1*. Prior to each atomization trial, the Gd metal was arc melted in an argon environment to produce a number of 100 g Gd “fingers” approximately 10 cm in length for better packing in the crucible. Arc casting also refines the Gd with respect to volatile impurities, such as Ca, which is used the reduction of rare earth fluorides or chlorides to the rare earth metals. Metals such as Ca will degrade the magnetic properties [6].

For magnetic measurements of the Gd prior to atomization, the arc melted Gd was used. The arc-melted Gd ingot was cut and shaped to produce a high aspect ratio rectangular prism (~0.70 x 0.85 x 4.9 mm³) for magnetic measurements.

With the lower reported purity, pre- and post-melt oxygen, nitrogen, and carbon impurity analysis was conducted using (LECO) inert gas fusion analysis (LECO ON-836 for O/N and LECO CS-844 for C). The as purchased stock gadolinium had moderate levels of oxygen, nitrogen, and carbon at 1,000, 280, and 60 ppm, respectively. After arc melting in argon to produce the ingot sample, the Gd showed O, N, and C at 1,500, 260, and 90 ppm, respectively, revealing that the arc melting process did slightly increase impurity levels.

2.3

Magnetic Measurements

Magnetic properties and the MCE (magnetocaloric effect) were measured in a vibrating sample magnetometer calibrated with a nickel standard. Saturation magnetization was measured at 5 K under an applied field of 90 kOe (7179 kA/m). Magnetization was measured as a function of temperature from 50 K above the T_c to 50 K below T_c in fields ranging 0-20 kOe (1595 kA/m) in increments of 2.5 kOe (199 kA/m) and from 20-70 kOe (1595-5584 kA/m) in increments of 5 kOe (400 kA/m). From the low field data (1 kOe, 80 kA/m) the Curie temperature (T_c) was extrapolated from the inflection point to zero magnetization. To quantify the MCE, magnetic entropy change was determined using iso-field approach, which integrates the areas between M-T curves of different magnetic field following the relationship between magnetic entropy and magnetization and methods used by Neves Bez et. al [17].

$$\Delta S_M(T, \Delta H) = \mu_0 \int_{H_i}^{H_f} \left(\frac{\partial M}{\partial T} \right)_H dH \quad (2)$$

The adiabatic temperature changes and magnetic-field dependent heat capacities were measured and will be reported separately.

3 Results:

3.1

Powder Yield and distribution

With successful atomization of Gd, the powder was collected and characterized. The desired spherical powder diameter was 200 μm , with an allowed target range of 150-250 μm . For run RDA-1-48, a 1,300 g charge was loaded in the crucible of the RDA, and 1219 g of powder were collected from the oil bath. The remainder between these two amounts was froze out in the crucible and/or solidified on the disk. The collected powder was separated through a series of ASTM standard sieves with an oscillating sieve shaker and measurements indicated 32% of the collected powder was within the target range. *Figure 2* shows a particle size distribution of the collected powder measured using a Microtrac dynamic light scattering particle analyzer. The mean particle diameter (d_{50}) was 216 μm , just slightly above the target 200 μm . However, the bimodal distribution of the powder suggests the atomization conditions were not ideal, lowering the yield in the target range.

In addition to size distribution, powder morphology was analyzed. *Figure 3(a)* shows the 150-250 μm powder as-sieved. While mostly spherical, there was a nontrivial fraction of off-round particles. To keep the porosity of the magnetic layers in the AMR at the intended design, the non-spherical particles (henceforth referred to as flake) were separated from the spherical powders. This separation was accomplished with a tilted rotating plate apparatus, similar in principle to those used by Riley [18] and Klar [19] and designed with help from collaborators at Pacific Northwest National Lab [20]. The slight angle of the plate was used to roll spheres off one side of the plate while flake remained in place and was swept off with blowing air on the opposite side, separating spherical powder and flake into different reservoirs. This process revealed the total flake content in the 150-250 μm range to be 12%. *Figure 3 (b) and(c)* show the separated flake

and spherical powders, respectively. By this means, a total of 350 g of spherical powder was produced.

3.2

Magnetic Properties

The Gd ingot sample showed a saturation of 264 emu/g ($264 \text{ Am}^2/\text{kg}$) under 90 kOe (7179 kA/m) at 5 K. The T_c was extrapolated from magnetization data to be 294 K (289 K from maximum entropy change)., This T_c falls at the lower range of reported values for other commercial grade Gd ranging from 289-295K [6], likely resultant of the higher impurity content of the commercial grade material. The magnetic entropy changes in various fields calculated from the magnetization data are provided in *Figure 4*. The plots show a maximum ΔS_m of 4.3, 7.3, 9.9 and 12.1 J/kg K in applied fields of 1, 3, 5, and 7 T, respectively, for the ingot sample. The powder sample shows a lower ΔS_m with a drop between of 0.6-0.7 J/kg K for the various fields. While the 1 T calculation is on par with literature, these values are somewhat lower than what has been reported in other studies of high field magnetic entropy change in Gd [6, 8, 9]. In addition, the peak entropy change is shifted down to 289 K, near the lower range of reported peak ΔS_m . These changes in properties from the reported values of pure Gd are likely resultant of the lesser purity (Table 1) of the commercial Gd used in this experiment as it has been established that the T_c and MCE of Gd are reduced with lower purity [7, 12-14]. The Gd stock used in this work had reported high levels of both C and Ca as was seen in a low purity Gd sample reported by Dan'kov which also showed reduced magnetocaloric performance compared to high purity samples[6].

Total entropy curves for the Gd ingot sample were calculated using the calculated magnetic entropy change data with measured heat capacity of the Gd ingot sample in zero applied field allowing for determination of adiabatic temperature change with the method described by Pecharsky and Gschneidner [9]. The calculated plots shown in *Figure 5* reveals a maximum ΔT_{ad}

of 3.9, 7.0, 10.0 and 12.8 K in applied fields of 1, 3, 5, and 7 T, respectively. These values fall below the theoretical limits for Gd [21], but like the magnetic entropy change, the ΔT_{ad} at 1 T is near reported values in the literature while the higher field ΔT_{ad} values are slightly lower (~1K) than values reported on Gd with the same field changes [6, 7, 9]. Both the ingot and powder measurements show slightly shorter and narrower ΔS_m peaks compared to the higher purity single crystal Gd sample from Dan'kov et. al [6], both factors contributing to the reduction of ΔT_{ad} . showing loss of magnetic performance with lower purity [21]. While slightly suppressed, the cooling potential of this material used in the AMR is still significant. Due to the size and morphology, heat capacity measurements could not be obtained on the atomized powder, but it is predicted a similar trend would be seen to that of the ΔS_m i.e., powder performance slightly lower than the ingot values.

The magnetic saturation of the 150-250 μ m powder was measured to be 261 emu/g (261 Am²/kg) at 5 K under 90 kOe (7179 kA/m). The T_c extrapolated from magnetization data was 293 K (289 K from maximum entropy change). This is just slightly lower than the ingot value. The entropy change calculated from the isofield magnetization vs temperature data for the powder shows peak values lower than the ingot at all fields. The maximum ΔS_m in applied fields of 1, 3, 5, and 7 T were 3.6, 6.7, 9.3 and 11.5 J/kg K, respectively, for the powder sample (Figure 4). This is both a slight decrease in the T_c and the magnetic entropy change between ingot and powder indicative of additional impurity pickup during atomization.

4 Discussion:

4.1

Powder Yield

The atomization run discussed previously was successful in producing 350g of spherical powders between 150-250 μ m in diameter from a 1,300g charge, a 27% yield. The relatively low

yield can be attributed to three main losses: system loss, particle size distribution shift, and flake production.

The material loss to the system are comprised of freeze out in the crucible and freezing of the metal on the disk. The material left in the crucible was *43g (3% of the charge)*. This loss could potentially be prevented in future atomization attempts by better controlling heating of the crucible during the pour to prevent early solidification of the charge.

The bimodal particle size distribution of the powder also indicates loss of powder in the target size range. This distribution is indicative of inconsistent run parameters during atomization. For instance, if the initial pour was off center of the pin atop the disk assembly, a pulsed flow of liquid metal flows over the disk rather than a consistent sheet of atomizing liquid. To pinpoint the culprit, it would be useful to collect visual data through high speed video, an option unavailable at the time of this atomization. However, better ensuring consistencies such as charge flow rate and atomization conditions throughout the duration of the run will help ensure a uni-modal and narrow particle size distribution in the powder.

A nontrivial portion of the produced powder in the desired size range was irregular, flake-like particles (12%). It is posited that this flake is produced when spherodized droplets of the charge material are not substantially cooled before reaching the quench wall. If too hot, the particle may not keep its shape upon contact with the outer quench bath wall, deforming into a flake due to stress on impact. Therefore, it is important to ensure proper cooling time, i.e., adequate particle flight times, are available in the system. The flight time is constrained by the disk rotation (particle) speed and the diameter of the rotating quench bath. Adjusting disk speed to increase flight time (reducing disk speed), would shift the d_{50} higher according to (1), an undesirable effect for enhanced yield of the desired powder diameter.

Increasing flight time through expansion of the quench bath diameter has already been shown. The previously described atomization of Gd powder was performed in the Ames Laboratory RDA with an expanded quench bath from what is referenced by Tian et. al [11]. Before this expansion, atomization of rare earth metals under similar run conditions but with a 40% smaller quench bath diameter produced 30-50% flake in the 150-250 μ m size range. Therefore, it has been shown that providing adequate flight time to the particles by providing a longer flight path to the quench wall is effective in reducing flake production.

4.2

Magnetic properties

A major concern of atomizing rare earth metals is the pickup of additional impurity and resultant loss in magnetic performance. Good indicators of impurity induced magnetic degradation are the T_c and saturation. The ingot sample had $T_c=294$ K and $M_s=264$ emu/g while the powder showed $T_c=293$ K and $M_s=261$ emu/g. The good agreement in these properties indicates that the powder is magnetically similar to the source material, verifying that the rotating disk atomization process did not degrade the magnetic properties by a significant amount.

More indicative of the change of properties in specific to the AMR application is the reduction of ΔS_m in the powder compared to the ingot (Figure 4). This change may be resultant of a number of factors. A small part may be attributed to the difference in demagnetization fields. Whereas the ingot sample was made to be a parallelepiped with long aspect ratio ($N_z \sim 0.07$ [22]), the magnetization data for the powders was obtained from a loosely packed ($\sim 54\%$ dense) sample of spheres. Using the conclusions from Bjork [23], the demagnetization factor of the powder sample is estimated to be approximately 0.28, four times greater than the ingot sample. As shown by Bahl and Nielsen, the MCE of Gd can be significantly suppressed with demagnetization factor [24]. Consideration of the demagnetization factor could also explain the slight reduction of T_c

between the ingot and the powder samples [25]. However, the change in ΔS_m from ingot to powder does not change drastically between low and high field measurements (powder ΔS_m is less 0.6 J/kg K at 1T and 0.4 J/kg K at 7T) indicating the dependence on demagnetization is small.

A more significant contributor to the loss of ΔS_m is likely due to impurity pickup during atomization. While a full impurity analysis was not conducted for the powder, several key impurities were quantified through LECO analysis. The atomized spherical powder in the desired 150- 250 μm size range saw increases in O content from 1,500 ppm to 2,000 ppm while the C content increased from 90 to 385 ppm compared to the arc melted ingot. It has been previously seen that C impurity content can significantly affect the magnetothermal properties of Gd [6, 14]. With a more than four-times increase of carbon content in the powder, this impurity is likely a large contributor to the changes in magnetic performance between the ingot and powder samples. While the magnetic entropy change of both the powder and ingot were less than published values for Gd the relatively small loss of performance from ingot to powder ($<10\%$ ΔS_m in fields greater than 3 T) shows that the atomization technique used in this work is viable for producing spheres for a powder based AMR.

As purity affects the overall performance of the powder, it is important to note that the impurity pickup from the RDA process is dependent on the morphology and size of the powder collected. Comparing morphology in the targeted 150- 250 μm size spherical powder showed lower content of both O (2,000 ppm) and C (380 ppm) compared to the flake removed from the same size range (2,500 and 745 ppm, respectively). The increased impurities in the flake likely result from the greater surface area of these particles. While carbon content remains relatively constant between the 45- 150 μm , 150- 250 μm , and 250- 300 μm size ranges (365, 383, and 385 ppm, respectively) oxygen pickup is greater in the smaller size powder with O content of 3,100, 2,000, and 1,900 ppm in these size ranges, respectively. Since smaller spheres will have

a greater surface area to volume ratio, this trend may be partially attributed to O pickup on the surface from the quench oil.

5 Conclusions:

Gadolinium powder for use in an AMR was successfully produced using the techniques of centrifugal atomization on a rotating disk with a co-rotating quench bath using the Ames Laboratory RDA system. While overall spherical powder yield in the target size range was only 27%, the run provides insight into the RDA process for changes that can be made in future runs to mitigate system losses, narrow size distribution, and reduce non-spherical, flake, content. Furthermore, the magnetic properties of the charge material and produced powder were in good agreement, validating the RDA technique for producing spherical rare earth metal powders while maintaining high magnetic performance.

Acknowledgment

This material is based upon work supported by the U.S. Department of Energy's Office of Energy Efficiency and Renewable Energy (EERE). The specific organization overseeing this report is the Fuel Cell Technologies Office (FCTO) under Award Number HI-480012-19.

Table 1: Impurity content of the as received commercial Gd as reported by Hefa Rare Earth Canada Co. Ltd.

Impurity	Wt%
La	0.0025
Ce	0.0010
Tb	0.0012
Dy	0.0015
Ho	0.0020
Fe	0.0120
Ca	0.0450
C	0.0140
W	0.0550
Mn	0.0010

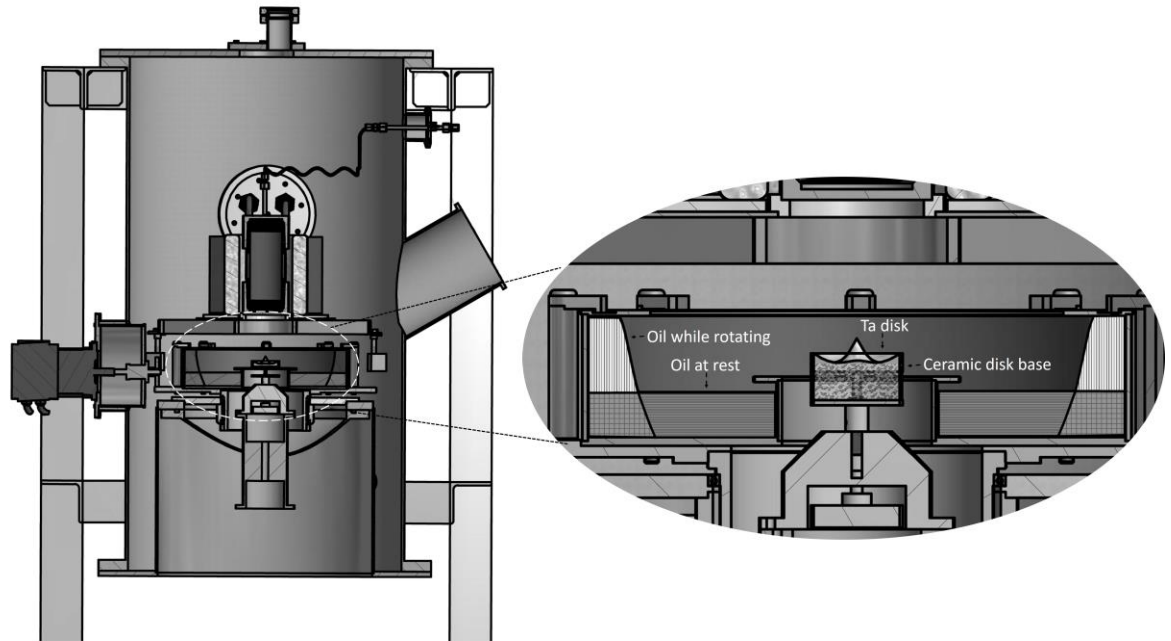


Figure 1: Rotating disk atomizer (RDA) at Ames Laboratory highlighting the co-rotating quench bath utilized to reduce flight distance required for the solidification of atomized metals

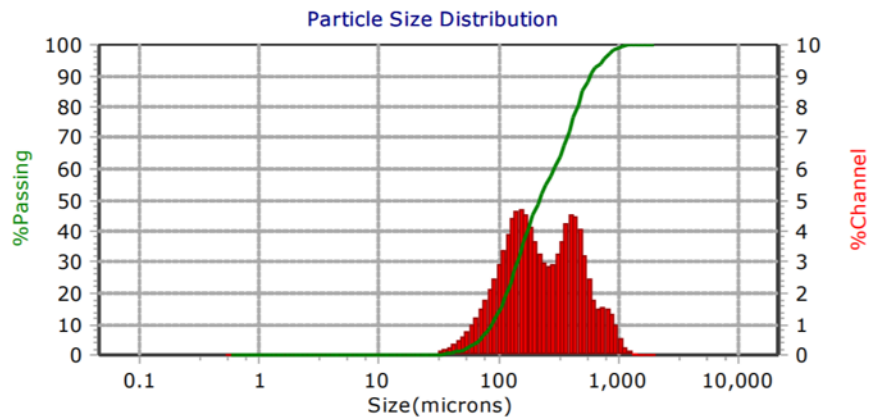


Figure 2: Particle size distribution in Gd powder showing d_{50} at $216\mu\text{m}$. Bimodal distribution indicative of non-ideal atomization conditions.

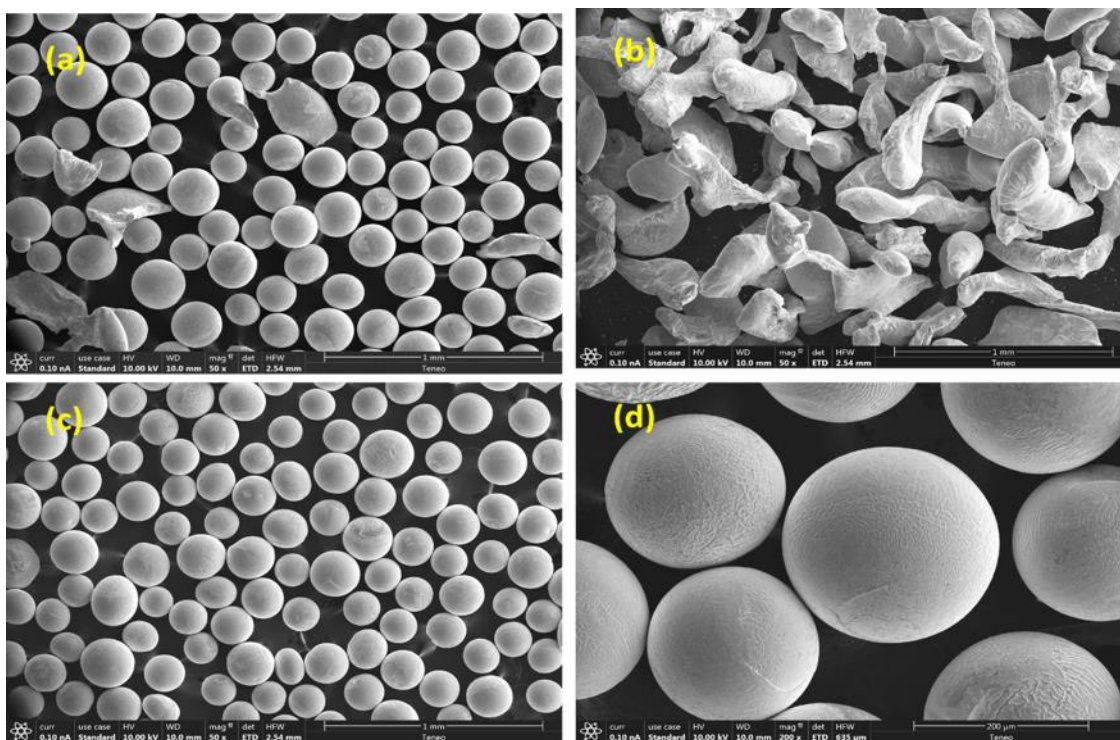


Figure 3: SEM micrographs of the Gd powder showing (a) as collected spheres with some flake, (b) separated flake, and (c,d) isolated spheres. The total flake content was 12%.

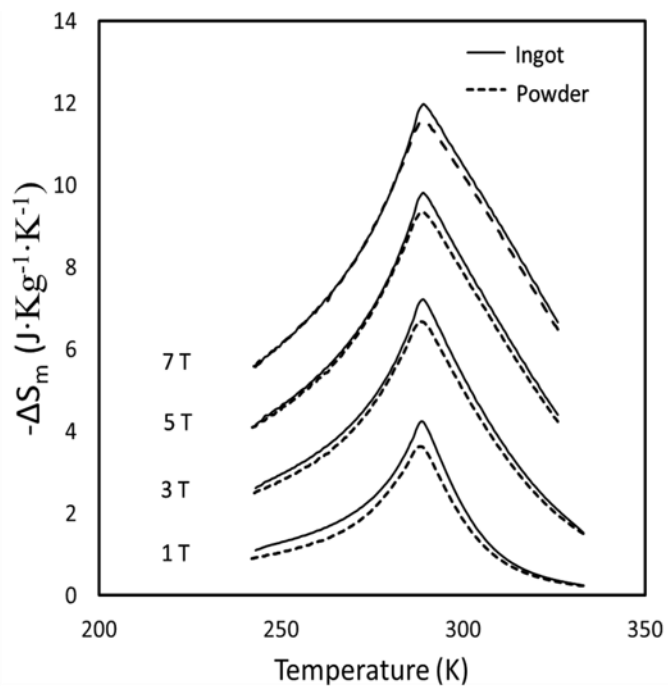


Figure 4: Magnetic entropy change of Gd ingot sample and powder sample in various fields.

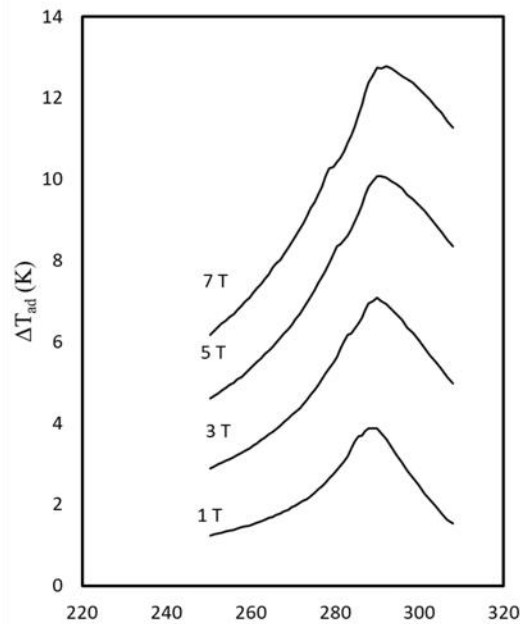


Figure 5: Adiabatic temperature change of the Gd ingot sample as a function of applied field. Values calculated from combined heat capacity and magnetization data.

- [1] K.A. Gschneidner, V.K. Pecharsky, Rare Earths and Magnetic Refrigeration, *Journal of Rare Earths*, 24 (2006) 641-647.
- [2] J. Barclay, W. A. Steyert, Active magnetic regenerator, 1982.
- [3] J. Holladay, R. Teyber, K. Meinhardt, E. Polikarpov, E. Thomsen, C. Archipley, J. Cui, J. Barclay, Investigation of bypass fluid flow in an active magnetic regenerative liquefier, *Cryogenics*, 93 (2018) 34-40.
- [4] R. Teyber, K. Meinhardt, E. Thomsen, E. Polikarpov, J. Cui, A. Rowe, J. Holladay, J. Barclay, Passive force balancing of an active magnetic regenerative liquefier, *Journal of Magnetism and Magnetic Materials*, 451 (2018) 79-86.
- [5] R. Teyber, J. Holladay, K. Meinhardt, E. Polikarpov, E. Thomsen, J. Cui, A. Rowe, J. Barclay, Performance investigation of a high-field active magnetic regenerator, 2019.
- [6] S.Y. Dan'kov, A.M. Tishin, V.K. Pecharsky, K.A. Gschneidner, Magnetic phase transitions and the magnetothermal properties of gadolinium, *Physical Review B*, 57 (1998) 3478-3490.
- [7] S. M. Benford, G. V. Brown, T - S diagram for gadolinium near the Curie temperature, 1981.
- [8] M. Foldeaki, R. Chahine, T. K. Bose, Magnetic measurements: A powerful tool in magnetic refrigerator design, 1995.
- [9] V.K. Pecharsky, K.A. Gschneidner, Magnetocaloric effect from indirect measurements: Magnetization and heat capacity, *Journal of Applied Physics*, 86 (1999) 565-575.
- [10] M. Osborne, I. E. Anderson, K. A. Gschneidner, M. J. Gailloux, T. Ellis, Centrifugal Atomization of Neodymium and Er₃Ni Regenerator Particulate, 1994, pp. 631-638.
- [11] L. Tian, I. Anderson, T. Riedemann, A. Russell, Production of fine calcium powders by centrifugal atomization with rotating quench bath, *Powder Technology*, 308 (2017) 84-93.

- [12] B. Champagne, R. Angers, SIZE DISTRIBUTIONS OF POWDERS ATOMIZED BY THE ROTATING ELECTRODE PROCESS, 1981.
- [13] T. Ishikawa, J. Okada, P.-F. Paradis, Y. Watanabe, Thermophysical Property Measurements of Liquid Gadolinium by Containerless Methods, 2010.
- [14] L.B. Robinson, F. Milstein, Effects of impurities on heat capacities at paramagnetic to ferromagnetic transitions, Solid State Communications, 13 (1973) 97-100.
- [15] L.W. Roeland, G.J. Cock, F.A. Muller, A.C. Moleman, K.A. McEwen, R.G. Jordan, D.W. Jones, Conduction electron polarization of gadolinium metal, Journal of Physics F: Metal Physics, 5 (1975) L233-L237.
- [16] K.A. Gschneidner Jr, Metals, alloys and compounds-high purities do make a difference!, 1993.
- [17] H. Neves Bez, H. Yibole, A. Pathak, Y. Mudryk, V.K. Pecharsky, Best practices in evaluation of the magnetocaloric effect from bulk magnetization measurements, Journal of Magnetism and Magnetic Materials, 458 (2018) 301-309.
- [18] G.S. Riley, An examination of the separation of differently shaped particles, Powder Technology, 2 (1969) 315-319.
- [19] E. Klar, Approaches to mechanical separation of materials, Powder Technology, 3 (1969) 313-314.
- [20] K. Meinhardt, E. Thomsen, T. Riedemann, Personal Communication, 2017.
- [21] V.I. Zverev, A.M. Tishin, M.D. Kuz'min, The maximum possible magnetocaloric ΔT effect, Journal of Applied Physics, 107 (2010) 043907.
- [22] A. Aharoni, Demagnetizing factors for rectangular ferromagnetic prisms, Journal of Applied Physics, 83 (1998) 3432-3434.
- [23] R. Bjørk, C.R.H. Bahl, Demagnetization factor for a powder of randomly packed spherical particles, Applied Physics Letters, 103 (2013) 102403.
- [24] C.R.H. Bahl, K.K. Nielsen, The effect of demagnetization on the magnetocaloric properties of gadolinium, Journal of Applied Physics, 105 (2009) 013916.
- [25] V.I. Zverev, R.R. Gimaev, A.M. Tishin, Y. Mudryk, K.A. Gschneidner, V.K. Pecharsky, The role of demagnetization factor in determining the 'true' value of the Curie temperature, Journal of Magnetism and Magnetic Materials, 323 (2011) 2453-2457.